THE JOURNAL OF BIOLOGICAL CHEMISTRY VOL. 288, NO. 6, pp. 4048–4059, February 8, 2013

LcrH, a Class II Chaperone from the Type Three Secretion System, Has a Highly Flexible Native Structure*[S]

Received for publication, June 28, 2012, and in revised form, December 7, 2012 Published, JBC Papers in Press, December 11, 2012, DOI 10.1074/jbc.M112.395889

Sunny K. Singh[‡§1], **Aimee L. Boyle**[¶2], **and Ewan R. G. Main**[‡3]

From the [‡]*School of Biological and Chemical Sciences, Queen Mary, University of London, London, E1 4NS, the* [§]*School of Life Sciences, University of Sussex, Falmer, near Brighton, BN1 9QJ, and the* [¶]*School of Chemistry, University of Bristol, Bristol, BS8 1TS, United Kingdom*

Background: Bacterial pathogens using the type III secretion system (T3SS) require class II chaperones (LcrH) for infection.
Results: The modular TPR fold of LcrH produces a weakly folded structure held together by its weak dimeric interface.
Conclusion: Under physiological conditions, LcrH populates partially folded structures, thus suggesting a mechanism for cargo binding.
Significance: This work is important for understanding one essential part of the T3SS.

The type three secretion system is a large and complex protein nano-machine that many Gram-negative pathogens employ to infect host cells. A key structure of this machine is a proteinaceous pore that inserts into the target membrane and forms a channel for bacterial toxins to flow from bacteria into the host cell. The pore is mainly formed from two large membrane proteins called "translocators." Importantly, effective secretion and thus pore formation of the translocators depend on their binding to and being transported by small specialized chaperones after synthesis in the bacterial cytosol. Recent crystal structures have shown these chaperones are formed from modular tetratricopeptide repeats. However, each crystal structure produced different homodimeric structures, suggesting flexibility in their topology that may be of importance to function. Given the crucial role of the translocator chaperones, we investigated the conformational stability of the chaperone LcrH (*Yersinia pestis*). Mutational analysis coupled with analytical ultracentrifugation and equilibrium denaturations showed that LcrH is a weak and thermodynamically unstable dimer ($K_D \approx 15\ \mu M$, $\Delta G_{H_2O} = 7.4$ kcal mol^{-1}). The modular tetratricopeptide repeat structure of the dimer allows it to readily unfold in a noncooperative manner to a one-third unfolded dimeric intermediate ($\Delta G_{H_2O} = 1.7$ kcal mol^{-1}), before cooperatively unfolding to a monomeric denatured state ($\Delta G_{H_2O} = 5.7$ kcal mol^{-1}). Thus, under physiological conditions, the chaperone is able to populate C-terminally unraveled partially folded states, while being held together by its dimeric interface. Such ability suggests a "fly-casting" mechanism as a route to binding their far larger translocator cargo.

Several pathogenic Gram-negative bacterial genera such as *Shigella, Yersinia,* and *Pseudomonas* use the type III secretion system (T3SS)[4] to deliver toxins directly into the cytosol of host eukaryotic cells (1–3). To achieve this, the T3SS forms a large multiprotein complex that produces a channel that directly links the bacterial cytosol to the host cell cytosol. The complex is composed of over 20 proteins that combine to form a basal structure that spans both bacterial membranes, a hollow needle-shaped structure that projects from the bacteria to the host cell, and a pore that forms on the tip of the "needle" and inserts into the eukaryotic cell membrane (1, 4, 5). The pore completes the channel from bacteria to host and is mainly composed of two large transmembrane domain-containing proteins (4–6). These are generally referred to as the "translocators" and have differing specific names depending on the bacteria from which they originate (for example, YopB and YopD in *Yersinia* spp. and IpaB and IpaC in *Shigella* spp., respectively).

Importantly, pore formation and thus infection can only occur when the translocators are bound by a small acidic specialized chaperone in the bacterial cytosol (termed class II chaperones) (7–10). The translocator-chaperone complex can then traffic to the tip of the needle where it dissociates to allow the pore to form (1). The significance of the translocator-chaperone complex to bacterial pathogenicity is easily highlighted by studies that show chaperone null bacterial strains are non-invasive to eukaryotic cells (8, 9). Excitingly, four crystal structures of translocator chaperones were recently solved as follows: SycD from *Yersinia enterocolitica*, IpgC from *Shigella flexneri*, and PcrH from *Pseudomonas aeruginosa* (7–9, 11, 12). The structures revealed the chaperones to be homodimers with a common all α-helical fold. This fold is composed of three tandemly arrayed tetratricopeptide repeats (TPRs) (Fig. 1 and supplemental Fig. 1). TPRs are short 34 amino acid motifs that adopt a helix-turn-helix conformation and stack on each other to form elongated structures.

* This work was supported in part by Queen Mary, University of London, and Sussex Universities.
[S] This article contains supplemental Materials and Methods, Figs. S1–S3, Scheme 1, Equations 1–7, and additional references.
[1] Supported by a Sussex University studentship.
[2] Supported by a Biotechnology and Biological Sciences Research Council studentship with Prof. Dek Woolfson.
[3] To whom correspondence should be addressed: School of Biological and Chemical Sciences, Queen Mary, University of London, Mile End Road, London, E1 4NS, UK. E-mail: e.main@qmul.ac.uk.

[4] The abbreviations used are: T3SS, type III secretion system; LcrH, low calcium response H; SEC, size exclusion chromatography; AUC, analytical ultracentrifugation; TPR, tetratricopeptide repeat; fl, full length; tr, truncated.

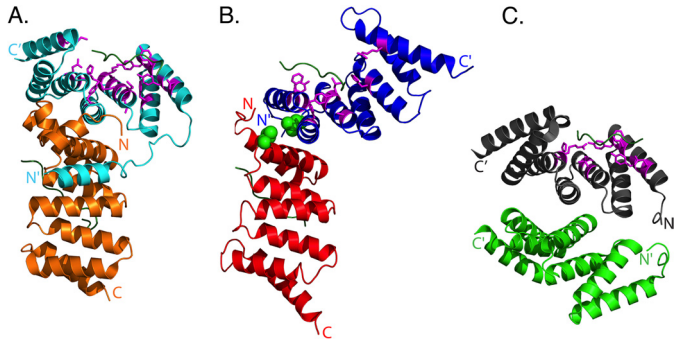

FIGURE 1. **Crystal structures of the class II chaperones of the type III secretion system.** *A, ribbon* representation of the asymmetric dimer IpgC(1–151) with bound peptides of IpaB (translocator protein) in back-to-head confirmation (Protein Data Bank code 3GZ1). Chain A and chain B of IpgC(1–151) are colored *cyan* and *orange*, respectively. The bound peptides of IpaB are colored *dark green*. Residues in chain A of IpgC that interact with IpaB are shown as *sticks* and are colored *purple*. These are located in TPR1–3. *B, ribbon* representation of the dimer SycD(21–163) with bound peptides of YopD(56–65) (translocator protein) in back-to-head confirmation (Protein Data Bank code 4AM9). Chain A and chain B of SycD(21–163) are colored *blue* and *red*, respectively. The bound peptides of YopD are colored *dark green*. Residues in chain A of SycD that interact with YopD are shown as *sticks* and are colored *purple*. These are located in TPR1–3. Leucine 65 is represented by *green spheres* and was mutated to glutamic acid to obtain monomeric protein. SycD differs from LcrH in only two positions (N136D and P138T, respectively). *C, ribbon* representation of PcrH(21–160) with the bound peptide of PopD (Protein Data Bank code 2XCB). Chain A and chain B of PcrH are colored *dark gray* and *green*, respectively. The bound peptides of PopD are colored *dark green*. Residues in PcrH that interact with PopD are shown as *sticks* and are colored *purple*. Figures *A–C* were prepared using PyMOL.

Interestingly, when the structures and accompanying biochemical characterizations are compared, a number of features are immediately apparent as follows. (i) Although biochemical studies have implicated more than one interaction between chaperone and translocator (7, 13, 14), structures of IpgC with IpaB(51–72), PcrH(21–160) with PopD(47–56), and SycD(21–163) with YopD(56–65) show a common main interaction site where an extended peptide from each translocator binds on the concave face of its cognate TPR domain (1:1 ratio) (Fig. 1). This suggests that the chaperone can only bind one translocator at a time.

(ii) Although class II chaperones are generally homodimeric, their exact mode of dimerization is somewhat ambiguous. The crystal structures provide a number of possible conformations depending on the protein and construct used (Fig. 1 and supplemental Fig. 1). For N-terminally shortened SycD(21–163) and IpgC(10–151), further mutational analysis suggested that a head-to-head dimer was the relevant unit (Fig. 1). In the case of SycD, crystal structures show two possible head-to-head conformations (supplemental Fig. 1, *A* and *B*). In contrast, the relevant unit of full-length IpgC(1–151) seems to be a back-to-head conformation. N-terminally shortened PcrH(21–160) crystal structures show two dimer structures that might be stable in solution, an asymmetric back-to-back dimer and a symmetric head-to-head dimer (supplemental Fig. 1, *E* and *F*).

(iii) To investigate the physiological role of class II chaperone dimerization, *in vivo* experiments were carried out in *Yersinia* and in *Shigella,* respectively. Here, the mutated monomeric mutant showed characteristics typical of a null mutant. These consisted of a lack of translocator secretion and an inability to invade mammalian cells (8, 9). Yet studies on AcrH and PcrH have shown that translocator binding disrupts their dimeric structures and produces 1:1 chaperone-translocator complexes (7, 15).

Such structural ambiguity suggests certain flexibility in the topology of the translocator chaperones, which would seem to be of importance to their function. This appears logical given the modular TPR units that form their structure. However, there is little information and no biophysical studies to have specifically investigated whether this is the case.

Therefore, in this study we have biophysically characterized the class II chaperone LcrH from *Yersinia pestis*. This is identical, except for two minor amino acid substitutions, to SycD from *Y. enterocolitica* (Fig. 1 and supplemental Fig. 1, *A* and *B*). We show that LcrH is a weak dimer ($K_D \approx 15\ \mu$M) that readily unfolds in a noncooperative manner to a partially unraveled dimeric intermediate. Furthermore, we show that although deletion of the N terminus does remove some α-helical structure ($\approx$10%), it does not affect either its stability or dimerization equilibrium. Excitingly, the energy barrier for the partial unraveling of dimeric LcrH is low ($\Delta G_{H_2O} \approx 1.7$ kcal mol^{-1} at 25 °C), suggesting that partially unfolded states of LcrH (held together at the dimeric interface) are present at physiological conditions. We propose that such a loosely folded structure has biological relevance, at the very least, when binding its cognate protein partners (the far larger membrane inserting translocator proteins).

EXPERIMENTAL PROCEDURES

Cloning, Expression, and Purification of LcrH and Truncated LcrH Proteins—The cloning, expression, and purification of full-length LcrH (fl-LcrH, 168 amino acids), the truncated LcrH (tr-LcrH, amino acids 21–163, 143 residues), and L65E variant proteins are described in detail in the supplemental Materials and Methods. LcrH and tr-LcrH have the same amino acid sequence, except for two amino acid substitutions, D136N and T138P, to SycD and the truncated form of SycD described in the crystal structure of the *Y. enterocolitica* gene of SycD, respectively (9). These mutations reside in a loop region between the last helix of the third TPR motif and a capping C-terminal helix (supplemental Fig. 1). The final protein purity of both LcrH and tr-LcrH was greater than 95% as measured by SDS-PAGE and UV absorption at 280 nm *versus* 260 nm. The final identity of the LcrH proteins was confirmed by MALDI mass spectrometry.

Biophysical Characterization of LcrH Proteins—In all experiments, 50 mM phosphate, pH 7.0, 5 mM DTT (LcrH buffer) was used. The molarity of the stock solutions of urea was determined using a refractometer (model NAR-1T, Atago, Tokyo, Japan).

Size Exclusion Chromatography (SEC)—SEC was performed on an ÄKTA FPLC system (GE Healthcare) by injecting 100 μl of protein at concentrations from 3 to 100 μM in LcrH buffer onto a Superdex^{TM} 75 10/30 column. For the SEC experiments involving urea-denatured protein samples, the column and protein sample was pre-equilibrated (4 h) and run with the required concentration of urea.

Analytical Ultracentrifugation (AUC)—Sedimentation equilibrium experiments were conducted using a Beckman-Optima

XL-I analytical ultracentrifuge fitted with an An-60 Ti rotor. Solutions were prepared at 40 μM protein concentration in LcrH buffer. Data were recorded at 25 °C using speeds in the range 17,000–30,000 rpm. Data were fitted to a model for a monomer-dimer equilibrium using the program Ultrascan (16). The partial specific volume of the peptide (0.7341 cm^3 g^{-1}) and the density of the solvent (1.0042 g cm^{-3}) were calculated using Sednterp (17). Errors were obtained by Monte Carlo analysis and given with 5% confidence limit.

Dynamic Light Scattering—Dynamic light scattering measurements were carried out using Zetasizer Nano S instrument (Malvern Instruments Ltd.). Samples were prepared at protein concentrations of 50 μM in LcrH buffer. For experiments involving urea-denatured protein samples, the protein sample was pre-equilibrated and run with the required concentration of urea. All samples were spun at 10,000 rpm for 10 min before taking measurements. The results were analyzed by Zetasizer software version 6.12 (Malvern Instruments Ltd.).

Circular Dichroism (CD) Spectroscopy—Far-UV CD was used to probe the secondary structure of the LrcH protein at different protein and denaturant concentrations. Spectra were acquired on either a Jasco J-715 or an Applied Photophysics Chirascan spectrophotometer. All far-UV CD spectra were acquired in LcrH buffer at 25 °C and using the following path lengths and protein concentrations: 1- or 5-mm path length for protein concentrations at 3 μM; 1-, 2-, or 5-mm path length for protein concentrations at 6, 12, and 25 μM, and 1-mm path length for protein concentrations at 50 and 80 μM. Spectra were recorded from 200 to 300 nm. To compare data, and thus correct for path length and concentration, all ellipticities were converted to molar ellipticity (degrees cm^2 $dmol^{-1}$).

Thermodynamic Stability (Equilibrium Denaturations)—Individual denaturation experiments were performed with LcrH using the protein concentrations and path lengths detailed above. At least two curves were recorded for each protein concentration to confirm reproducibility. For each denaturation experiment, a stock solution of urea was diluted to obtain a large range of denaturation concentrations using a Hamilton Microlab dispenser. LcrH protein and buffer were added to the differing denaturant concentrations to give identical protein (from 3 to 80 μM) and buffer concentrations (LcrH buffer). The length of time the experiments were left to equilibrate was determined by repeating a denaturation experiment after differing equilibration times (4, 8, 12, and 24 h). These all gave superimposable curves, showing that equilibrium was reached after 4 h (supplemental Fig. 2). Thus, all protein/denaturant solutions were pre-equilibrated at 25 °C for a minimum of 4 h prior to performing experiments on the CD. Scans were taken in a thermostatted cuvette holder at 25 ± 0.2 °C and between 210 and 250 nm at a scan rate of 1 nm s^{-1}. The largest difference in signal between native and denatured LcrH was observed at 222 nm, and this wavelength was used to monitor unfolding. For easy comparison of differing data sets, the signal at 222 nm (λ_{obs}) was converted to λ_{rel} (relative spectroscopic signal) using Equation 1,

$$\lambda_{rel} = \frac{(\lambda_{obs} - \lambda_N)}{(\lambda_D - \lambda_N)} \quad \text{(Eq. 1)}$$

where λ_N is the signal of the native state and λ_D is the signal of the denatured state.

RESULTS

Our studies were conducted on two constructs of the translocator chaperone LcrH from *Y. pestis* (99% identical to SycD from *Y. enterocolitica*). These consisted of the full-length protein termed fl-LcrH (comprising of 168 residues) and a truncated construct termed tr-LrcH (comprising of residues 21–163). The truncated construct matched the shortened version of SycD whose atomic structure was solved and permitted us to determine the effect of N-terminal deletion on the stability or conformational dynamics of the protein.

Structure of fl-LcrH and tr-LcrH in Solution—T3SS translocator chaperones in *Yersinia* and *Shigella* spp. have been shown to be homodimeric in solution (8, 9). However, no K_D value for the interaction has been published. To determine the oligomeric state of both forms of LcrH over a range of protein concentrations and to obtain a K_D value for the dimerization, SEC and equilibrium sedimentations by AUC were performed (Fig. 2). SEC showed that at high concentrations fl-LcrH and tr-LcrH elute with a single peak profile that is consistent with a homodimeric structure (elution volume of 9.7 and 9.6 ml, respectively, which is in close agreement with an elution peak of 9.6 ml obtained for a designed TPR protein containing 6.5 stacked repeats (this protein has similar dimensions to a head-to-head dimeric SycD)). Yet, when lowered to more physiological concentrations (from 100 to 3 μM), both elution peaks were observed to shift to that of a monomeric sized protein (Fig. 2). For example, tr-LcrH at 3 μM elutes with a peak of 10.7 ml, which is in close agreement with an elution peak of 10.7 ml for the monomeric L65E tr-LcrH mutant and 10.55 ml obtained for a designed TPR protein containing 3.5 stacked repeats (a protein that has similar dimensions to monomeric SycD) (supplemental Fig. 2). The change in elution profile shows that LcrH is present in monomer-dimer equilibrium at physiological protein concentrations and therefore has a relatively weak dimerization interaction. It also suggests that its K_D value should be in the low micromolar range.

To determine the exact dissociation constant for this equilibrium, sedimentation by analytical ultracentrifugation was performed (Fig. 2*C*). This gave a dimerization dissociation constant, K_D, of 15 μM ± 5 for tr-LcrH. This confirms the relatively weak dimerization interaction of LcrH. From these data, the percentage of the protein population that is dimeric at any given total protein concentration can be calculated. These indicate that even at lower concentrations of protein there is dimer present. For example, at 1 and 3 μM, ~10 and 20% exist in the dimeric form, respectively.

LcrH Loses α-Helical Structure on N-terminal Deletion and Concentration Reduction—As LcrH is a completely α-helical protein, far-UV circular dichroism (far-UV CD) provides an excellent probe for monitoring its secondary structure in solution. Under our conditions, both fl-LcrH and tr-LcrH exhibit strong α-helical signals with indicative minima at 208 and 222 nm (Fig. 2, *A* and *B*). Interestingly, we observe a reduction in this signal (molar ellipticity at 222 nm) when tr-LcrH is compared with fl-LcrH and when the concentration of each protein

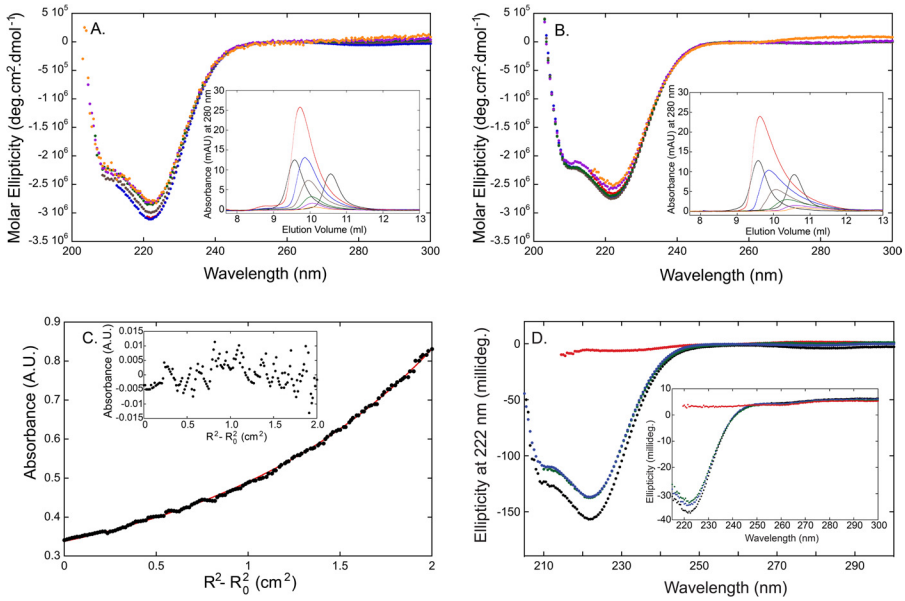

FIGURE 2. **Oligomeric state and structure of LcrH proteins.** *A* and *B,* far-UV CD spectra showing molar ellipticity from 200 to 300 nm for native fl-LcrH (*A*) and tr-LcrH (*B*) at concentrations of 100 μM (*red*), 50 μM (*blue*), 25 μM (*brown*), 12 μM (*green*), 6 μM (*purple*), and 3 μM (*orange*). The *insets* show the corresponding analytical size exclusion profiles for each LcrH concentration using a Superdex 75 HR 10/30 analytical gel filtration column. To calibrate the elution profiles, two standards were also run. These were CTPRa6 (a designed TPR protein that contains 6.5 continuously arrayed TPR motifs and thus should elute with a similar size to the dimeric LcrH) and CTPR3 (a designed TPR protein that contains 3.5 continuously arrayed TPR motifs and thus should elute with a similar size to the monomeric LcrH). Both are colored *black* with CTPRa6 having an elution peak of 9.6 ml and CTPR3 having an elution peak of 10.55 ml. *C,* representative curves obtained from equilibrium analytical ultracentrifugation for tr-LcrH. The figures show the data (*black circles*) and the line of best fit to a model for a monomer-dimer equilibrium using the program Ultrascan (*red*). The fitting residual is shown as the *inset*. *D,* far-UV CD spectra comparing native fl-LcrH (*black*), tr-LcrH (*blue*), L65E (*green*), and denatured L65E in 8 M urea (*red*). A protein concentration of 50 μM in a 1-mm path length was used in each experiment. The *inset* figure shows the same experiments conducted at a protein concentration of 3 μM in a 5-mm path length. Note that fl-LcrH has ~10% greater α-helical signal to tr-LcrH and L65E at 222 nm.

is decreased (Fig. 2 and supplemental Fig. 2). In each case, the change is small as follows: at 50 μM, fl-LcrH and tr-LcrH have molar ellipticities at 222 nm of -3.1×10^6 and -2.7×10^6 degrees cm^2 dmol^{-1}, respectively, and at 3.1 μM, fl-LcrH and tr-LcrH have molar ellipticities at 222 nm of -2.8×10^6 and -2.5×10^6 degrees cm^2 dmol^{-1}, respectively. In both comparisons, this equates to a maximal change of ≈10%. The reduction of α-helical signal from fl-LcrH to tr-LcrH suggests that the N-terminal 20-amino acid deletion of LcrH removes some α-helical structure. The loss of the α-helical signal with a decrease in protein concentration is consistent with the weak monomer/dimer equilibrium, *i.e.* lowering the concentrations of LcrH results in a monomeric state that is less α-helically structured than the dimer.

Equilibrium Unfolding and Thermodynamic Stability of LcrH—To determine the flexibility and thermodynamic stability of fl-LcrH and tr-LcrH, equilibrium chemical denaturation experiments were performed by unfolding each protein with urea at 25 °C and pH 7. The unfolding was followed by monitoring the change in far-UV CD signal at 222 nm (α-helical secondary structure). For each protein, chemical denaturations were conducted at a number of different protein concentrations. For fl-LcrH, these were 3 and 50 μM, and for tr-LcrH, these ranged from 1 to 80 μM (Fig. 3). Importantly, all denaturations were completely reversible and corresponded to transitions from an α-helical native state to an unstructured monomeric denatured state that lacked any residual secondary structure (Figs. 2*D* and 3 and supplemental Fig. 2). Reproducibility of each denaturation was confirmed by repeating each experiment at least once (supplemental Fig. 3). When the differing equilibrium denaturations were compared, the following features and trends were immediately apparent (Fig. 3, *A–D*).

Biphasic Denaturations Show LcrH Unfolds via Partially Folded Dimeric Intermediate—The profile of each equilibrium denaturation and its protein concentration dependence delineates the mechanism by which oligomeric proteins unfold. Such concentration dependence is a unique characteristic of oligomeric protein systems and is a direct consequence of protein unfolding being coupled with oligomeric dissociation. Once determined, the data can be fit to the correct dimer denaturation model and thus obtain the thermodynamic stability of the protein.

For both forms of LcrH, the denaturation profile of each protein concentration consisted of two transitions, an observation that becomes clearer with increasing protein concentrations. Initial unfolding produces a first sloping transition that accounts for the loss of approximately a third of the native α-helical signals (Fig. 3, *A–D*). This ends at a saddle point at ≈3 M urea. At higher denaturant concentrations, a second sharper transition was observed. This results in the complete unfolding of the protein at urea concentrations of greater than 6 M. The biphasic unfolding shows that a stable partially structured intermediate is populated during the unfolding of LcrH. Significantly, the first transition is concentration-independent, and the second transition is concentration-dependent (the midpoint shifts to higher urea concentration with an increase in protein concentration). The observed pattern of unfolding (protein concentration-independent first transition to a stable

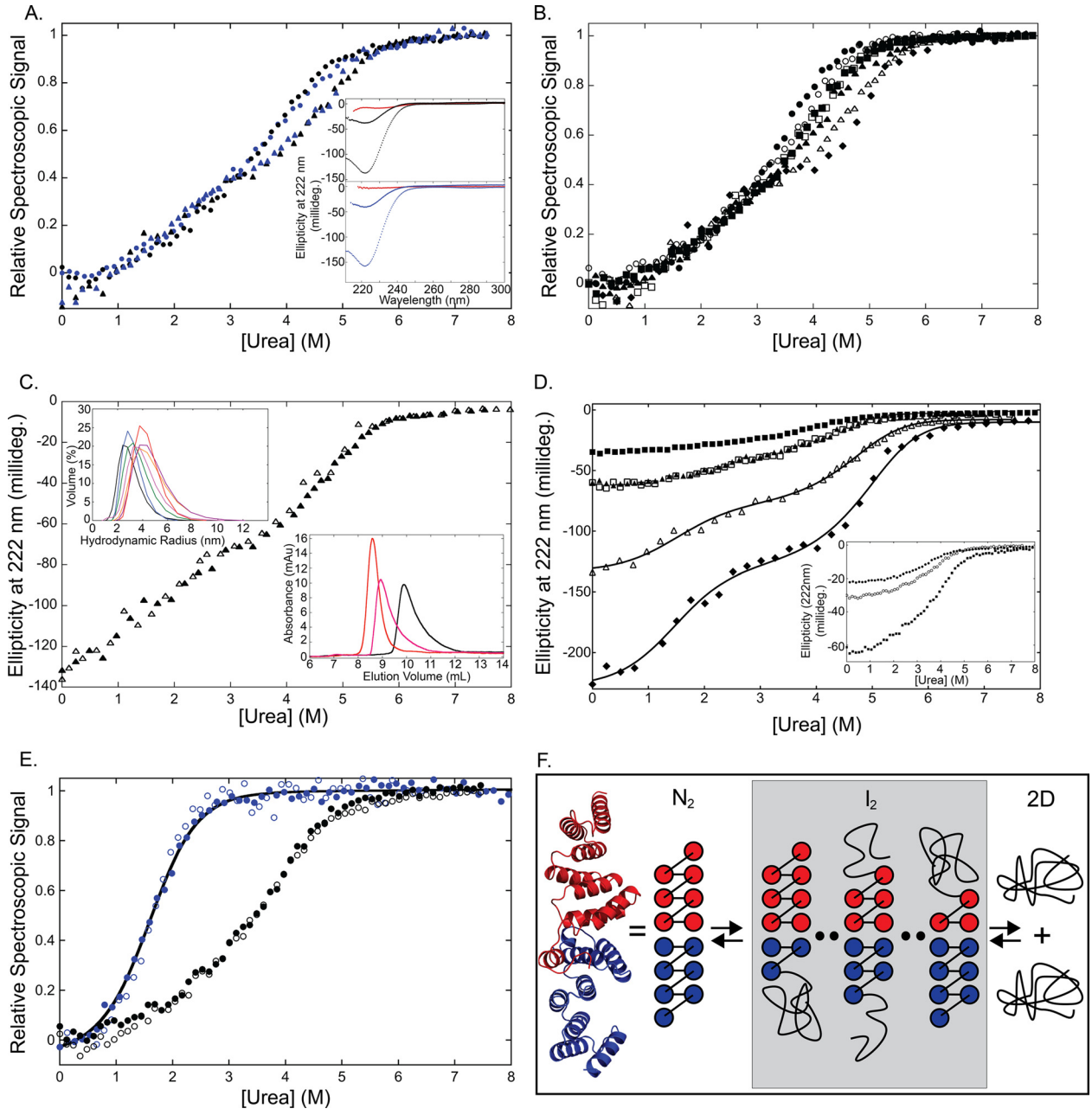

FIGURE 3. **Urea equilibrium denaturations of LcrH proteins and schematic of the unfolding pathway.** *A,* urea denaturations of fl-LcrH and tr-LcrH monitored by changes in far-UV CD at 222 nm and converted to relative spectroscopic signal (see Equation 1). For clarity, only one denaturation is shown per concentration: 3 μM (fl-LcrH, *blue-filled circles*; tr-LcrH, *black-filled circles*) and 50 μM (fl-LcrH, *blue-filled triangles*; tr-LcrH, *black-filled triangles*). The *lower right-hand inset* shows far-UV CD spectra comparing native *versus* denatured tr-LcrH and fl-LcrH at 50 μM (1-mm path length) and 3 μM (5-mm path length). (The same symbols are used as in the main figure, with the denatured protein traces colored *red*). *B,* urea denaturation of tr-LcrH monitored by changes in far-UV CD at 222 nm and converted to relative spectroscopic signal (Equation 1). For clarity only one denaturation is shown per concentration −1 μM (*filled circles*), 3 μM (*open circles*), 6 μM (*filled squares*), 12 μM (*open squares*), 25 μM (*filled triangles*), 50 μM (*open triangles*), and 80 μM (*filled diamonds*). *C,* urea denaturation of 50 μM tr-LcrH monitored by changes in far-UV CD at 222 nm (two data sets are shown, *open* and *closed triangles*). (i) The *upper left inset* shows dynamic light scattering of 50 μM tr-LcrH (volume of protein (%) against the hydrodynamic radius (nm)) when in 0 M urea (*black*), 1 M urea (*blue*), 2 M urea (*green*), 3 M urea (*pink*), 4 M urea (*orange*), 5 M urea (*purple*), and 6 M urea (*red*). (ii) The *lower right-hand inset* shows the analytical size exclusion chromatography of 50 μM tr-LcrH when in 0 M urea (*black*), 3 M urea (*pink*) and 6 M urea (*red*). *D,* urea denaturation of tr-LcrH monitored by changes in far-UV CD at 222 nm showing the global fit of the 50 and 80 μM data sets to a three-state model with a dimeric intermediate (supplemental Equation 4). For clarity, only one denaturation is shown per concentration, and these are divided between the main figure (6, 12, 25, 50, and 80 μM) and *inset graph* (1, 3, and 6 μM). The difference in signal between 6 μM datasets is due to collecting the data using differing path length cuvettes. Symbols are the same as in *B*. *E,* urea denaturation of LE65 mutant of tr-LcrH (*open blue circles,* 1.5 μM, and *filled blue circles,* 3 μM) and tr-LcrH at 3 μM (*black open* and *filled circles* for comparison) monitored by changes in far-UV CD at 222 nm and converted to relative spectroscopic signal (see Equation 1). The best fit for LE65 to a two-state folding model is shown (*black*). *F,* schematic illustration of the proposed equilibrium unfolding pathway of LcrH. A head-to-head dimeric structure of SycD (Protein Data Bank 2VGX) is shown next to a topological map of the fold for reference (helices are shown as *circles* with the individual protein chains colored *red* and *blue*). During unfolding, the native state (N_2) noncooperatively frays through unfolding of the C-terminal helices. This leaves an N-terminal dimeric intermediate (I_2). We note that various partially unfolded dimeric intermediate conformations could be populated during the unfolding transition. These are presented by showing the two extreme possible examples (one monomer of the dimer fully folded and the other mostly unfolding) and a third that is the median (both subunits partially unfolded to the same extent). These possible intermediate structures are shown in the *gray box*. At higher concentrations of urea the intermediate dissociates and denatures to a monomeric denatured state (*2D,* where D is the denatured state).

partially folded intermediate followed by a protein concentration-dependent second transition) is consistent with a scheme where native dimer (N_2) partially unfolds to a dimeric intermediate (I_2), which then unfolds to denatured monomer (2D), $N_2 \rightleftharpoons I_2 \rightleftharpoons 2D$ (Fig. 3*F*) (18). This pattern can be observed more clearly in Fig. 3*B* with tr-LcrH as chemical denaturations over a wider concentration range of 1–80 μM were possible (tr-LcrH remains aggregation-free at higher protein concentrations unlike fl-LcrH). Moreover, it is important to note that the shallow nature of the first unfolding transition, native dimer to partially unfolded intermediate, shows a lack of cooperative unfolding. This indicates the structure of LcrH is particularly flexible and can easily adopt partially unfolded conformations.

To confirm the dimeric intermediate unfolding mechanism, analytical SEC and dynamic light scatterings of tr-LcrH at 50 μM were performed in urea concentrations of 0–6 M urea. Both methods showed that there was an increase in the size of tr-LcrH on increasing urea concentrations (*insets,* Fig. 3*C*). In particular, the size of tr-LcrH was similar from 0 to 2 M urea but then significantly increased in 3 M urea. This shows that the first unfolding transition of LcrH involves partial unfolding to an expanded dimeric intermediate. By 6 M urea, the size of tr-LcrH had increased again through complete denaturation of the protein, with the shape of the peak by SEC becoming more symmetric. This shows that further unfolding produced an expanded monomeric species.

Deletion of N Terminus Causes No Change in Equilibrium Unfolding—When the equilibrium denaturations of fl-LcrH and tr-LcrH are compared at 3 and 50 μM, their profiles are indistinguishable (Fig. 3*A*). It is therefore clear that fl-LcrH and tr-LcrH have identical thermodynamic equilibrium unfolding and thus must unfold via the same mechanism and have the same stability. This shows that although the N terminus of LcrH may possess some α-helical content, it does not alter the conformational stability or the nature of equilibrium unfolding of the protein.

Thermodynamic Stability of LcrH—Having delineated the precise mechanism of LcrH unfolding, the thermodynamic stabilities of the intermediate and native states were obtained by globally fitting the chemical denaturations performed at 50 and 80 μM for tr-LcrH and 50 μM for fl-LcrH to a three-state unfolding model with a dimeric intermediate (Fig. 3*D*). The derivation of the three-state unfolding model and equations used to fit the data are described in detail in the data analysis section of the supplemental material. Lower protein concentration denaturations were excluded, as the intermediate state was not sufficiently populated to enable explicit fitting.

The thermodynamic parameters obtained are presented in Table 1 and confirm the identical stabilities of fl-LcrH and tr-LcrH. These show that the initial unfolding step ($N_2 \rightleftharpoons I_2$) has a $\Delta G^{N2 \rightleftharpoons I2}_{H2O}$ of only 1.7 ± 0.4 kcal mol^{-1}. Thus, the majority of the LcrH stability resides in the dimerization structure ($I_2 \rightleftharpoons 2D$), as it requires an extra 5.7 ± 1.2 kcal mol^{-1} to unfold. This means the total stability of the protein ($\Delta G^{N2 \rightleftharpoons 2D}_{H2O}$) is 7.4 ± 1.3 kcal mol^{-1}. Interestingly, LcrH's stability ($\Delta G^{N2 \rightleftharpoons 2D}_{H2O}$) is less than many other dimeric proteins that have been shown to unfold via dimeric intermediate (Table 2) (19). In particular, the first transition ($N_2 \rightleftharpoons I_2$) of LcrH was significantly lower than, for example, eAATase, Ure2p, SecA, OPH, and AAO proteins. This confirms the noncooperative and labile nature of LcrH's initial unfolding.

TABLE 1

Thermodynamic parameters for the global fitting of fl-LcrH and tr-LcrH at 25 °C using the three-state dimer model with a dimeric intermediate

Errors given are from the fit of all the data and are quoted at a 95% confidence level (two standard errors).

Global parameters					
protein	$\Delta G^{N_2 \rightleftharpoons I_2}_{H_2O}$ (kcal mol^{-1})	$m_{N_2 \rightleftharpoons I_2}$ (kcal mol^{-1} M^{-1})	$\Delta G^{I_2 \rightleftharpoons 2D}_{H_2O}$ (kcal mol^{-1})	$m_{I_2 \rightleftharpoons 2D}$ (kcal mol^{-1} M^{-1})	[a] $\Delta G^{N_2 \rightleftharpoons 2D}_{H_2O}$ (kcal mol^{-1})
fl-LcrH	1.7 ± 0.5	1.0 ± 0.3	5.6 ± 1.8	1.7 ± 0.4	7.3 ± 1.9
tr-LcrH	1.7 ± 0.4	1.1 ± 0.2	5.7 ± 1.2	1.7 ± 0.2	7.4 ± 1.3
Individual parameters					
	[Total Protein] (μM)	[b] λ_N (millideg.)	[c] λ_I (millideg.)	[d] λ_D (millideg.)	Cuvette pathlength (cm)
fl-LcrH	50 * 1	-99 ± 5	54 ± 6	-5 ± 2	0.05
fl-LcrH	50 * 2	-95 ± 5	54 ± 6	-5 ± 2	0.05
tr-LcrH	50 * 1	-132 ± 5	-73 ± 6	-4 ± 2	0.1
tr-LcrH	50 * 2	-133 ± 5	-70 ± 6	-3 ± 2	0.1
tr-LcrH	80 * 1	-226 ± 8	-126 ± 9	-9 ± 3	0.1
tr-LcrH	80 * 2	-206 ± 7	-122 ± 8	-14 ± 4	0.1

[a] $\Delta G^{N2 \rightleftharpoons 2D}_{H2O} = \Delta G^{N2 \rightleftharpoons I2}_{H2O} + \Delta G^{I2 \rightleftharpoons 2D}_{H2O}$, with the error calculated by propagating the fitting errors.
[b] λ_N is the CD spectroscopic signal for native LcrH at 222 nm.
[c] λ_I is the CD spectroscopic signal for intermediate LcrH at 222 nm.
[d] λ_D is the CD spectroscopic signals for denatured LcrH at 222 nm.

An apparent K_D (K_D^{app}) for the dissociation of the intermediate to denatured monomer can also be calculated from the equilibrium denaturation data. As $\Delta G^{I2 \rightleftharpoons 2D}_{H2O}$ (from the second unfolding transition) is the free energy of unfolding and dissociation of the intermediate LcrH to denatured monomeric LcrH, it is related to the K_D^{app} by $\Delta G^{I2 \rightleftharpoons 2D}_{H2O} = -RT\ln K_D^{app}$. Thus, K_D^{app} can be simply obtained by rearranging this equation (see supplemental Data Analysis). However, two caveats need to be considered before delineating its true significance. (i) K_D^{app} corresponds to both unfolding and dissociation of the intermediate state of LcrH. This is not exactly equivalent to the K_D value obtained from the SEC and AUC data, which correspond to the dissociation of folded dimeric LcrH to folded monomeric LcrH. (ii) the K_D^{app} is obtained in different solution conditions (high urea concentration). Given these caveats, the K_D^{app} calculated was 65 ± 65 μM and is consistent with the K_D calculated from AUC data and inferred from SEC data.

Proposed Equilibrium Unfolding Pathway—The ability of LcrH to easily fray into partially folded structures is facilitated by its modular TPR structure. Unlike globular proteins, TPR and other repeat-containing proteins are formed from the stacking of modular secondary structure motifs (Fig. 1) (20, 21). This causes their native structures to be dominated and stabilized by interactions from amino acid residues that are close in primary sequence, whereas globular proteins have many stabilizing interactions from amino acids that are distant in primary sequence. This arrangement can enable sections of repeat proteins to unravel without unfolding the complete structure. We have studied the folding of a number of designed TPR proteins and shown that when partial unfolding occurs, the proteins tend to unravel from the less stable outer repeats first (22–24). As the N termini of LcrH form the dimeric interface (which our results show is the most thermodynamically stable part of the structure), the unraveling must occur mainly from the C terminus. A schematic diagram of the equilibrium unfolding pathway proposed by our results is shown in Fig. 3*F*.

TABLE 2
Thermodynamic parameters characteristic of chemical-induced unfolding of dimeric proteins by a three-state transition with dimeric intermediate

Protein	Temp.	$\Delta G^{N2 \rightleftharpoons I2}_{H2O}$	$m_{N2 \rightleftharpoons} I2$	$\Delta G^{NI2 \rightleftharpoons 2D}_{H2O}$	$m_{I2 \rightleftharpoons} 2D$	$\Delta G^{N2 \rightleftharpoons 2D}_{H2O}$[a]
	°C	kcal mol^{-1}	kcal mol^{-1} M^{-1}	kcal mol^{-1}	kcal mol^{-1} M^{-1}	kcal mol^{-1}
tr-LcrH	25	1.7	1.1	5.7	1.7	7.4
eAATase[b]	25	12.0	4.8	24.4	3.4	36.4
SecA[c]	20	8.4	4.1	14.1	1.5	22.5
OPH[d]	25	4.3	1.0	36.1	4.3	40.4
AAO[e]	10	3.5	1.7	13.6	1.2	17.1

[a] $\Delta G^{N2 \rightleftharpoons 2D}_{H2O} = \Delta G^{N2 \rightleftharpoons I2}_{H2O} + \Delta G^{NI2 \rightleftharpoons 2D}_{H2O}$. To give the best comparison with our data on LcrH, the proteins chosen in this table were selected as the experimental conditions used to obtain them were similar to ours, *i.e.* urea as chemical denaturant, CD or fluorescence globally fitted, temperature between 10 and 25 °C, and pH between 7 and 8.
[b] The values quoted for eAATase are from Ref. 32.
[c] The values quoted for SecA are from Ref. 33.
[d] The values quoted for OPH are from Ref. 34.
[e] The values quoted for AAO are from Ref. 35.

Monomeric L65E tr-LcrH—To complete the stability studies conducted on LcrH, the stability and flexibility of the monomeric mutant L65E LcrH was investigated. *In vivo* studies have shown that when SycD is made monomeric through the L65E mutation, noninvasive bacteria are produced (9). This suggests that the dimeric interface is important for function. When we produced L65E tr-LcrH, we also obtained a monomer (at 50 μM there is a single SEC elution peak of 10.7 ml, which is similar to an elution peak of 10.55 ml obtained for a monomeric designed TPR protein of similar dimensions (3.5 stacked TPRs), supplemental Fig. 2*A*). Furthermore at 25 °C, L65E has same α-helicity by CD to dimeric tr-LcrH (Fig. 2*D*). However, chemical denaturation of L65E shows that the mutant was substantially destabilized compared with dimeric tr-LcrH with a single sharp transition between native and denatured states and little native base line (Fig. 3*E*). This was confirmed, as fitting the data to a two-state model showed the midpoint of the transition ($[D]_{50\%}$) is only 1.6 ± 0.1 M urea; the *m*-value of the transition is 1.4 ± 0.1 kcal mol^{-1} M^{-1}, and thus its stability ($\Delta G^{N \rightleftharpoons D}_{H2O}$) is 2.1 ± 0.2 kcal mol^{-1} ($\Delta G^{N \rightleftharpoons D}_{H2O} = m \cdot [D]_{50\%}$). This stability is similar to the initial unfolding of the dimer tr-LcrH, but it is substantially more cooperative and results in a complete loss of structure. Moreover, the low stability of L65E indicates that the *in vivo* results may well be caused by destabilizing LcrH to the extent that the monomers produced are unfolded and thus nonfunctional.

DISCUSSION

The biophysical data presented here highlight four key and exciting solution properties of the translocator chaperone LcrH that expand our understanding from the published crystal structures. First, both full-length and truncated LcrH proteins possess the same weak monomer-dimer equilibrium (low μM K_D), thermodynamic, and conformational stability. This shows that even though the removed N terminus possesses some α-helical structure, it does not affect the stability or conformational dynamics of the protein. Second, the thermodynamic barrier to partial unfolding is very low and occurs in a less than cooperative manner. This should cause populations of C-terminally unfolded structures to exist at physiological conditions. Third, when the dimer is formed, the interface provides added thermodynamic stability to the surrounding structure. This results in the dimeric interface and surrounding α-helices remaining folded at equilibrium when other parts of the structure can sample unfolded conformations. Finally, the monomeric mutant L65E is substantially destabilized in comparison with the wild-type dimer, but it unfolds in a more cooperative two-state manner.

Does the N Terminus Affect Dimer Orientation?—As discussed in the Introduction, a number of N-terminally truncated class II chaperones, for example SycD(21–163) and IpgC(10–151), produce head-to-head dimers. However, full-length IpgC forms a back-to-head dimer. Consequently, it has been suggested that the N terminus might be important for determining the arrangement of the subunits within the dimer structure. If this were the case, removing the N terminus should change the stability of the protein. However, for LcrH, removing the N terminus has no effect on stability. Therefore, it is unlikely that its dimeric structure changes on truncation. This implies that for LcrH at least the N terminus should not determine subunit positioning within the dimer. It would be interesting to determine whether this is the same for other class II chaperones.

Biological Relevance—It is the first five N-terminal α-helices of the class II chaperone proteins like LcrH that have been shown to form a significant portion of the binding interface with their cognate binding partners (the large membrane translocator proteins YopB and YopD for LcrH) (Fig. 1). These interactions primarily involve the class II chaperone binding an extended peptide between 10 and 20 residues of the translocator proteins, which maintain a molten globular form when in complex (7, 8, 11). The peptides each bind to a similar region of the concave groove formed by all three TPR motifs. Additionally, a recent study shows that the translocator chaperones may also bind supplementary regions on the translocator proteins as well (7, 13, 14). However, the mechanism by which these small chaperones find their cognate peptide sequences within the structure of the large membrane translocator proteins remains unclear.

Excitingly, these results support one possible mechanism, termed "fly-casting," by which these class II chaperones could operate. Here, the weakly folded C-terminal repeats of the chaperone adopt unfolded conformations that allow them to more easily find the target peptide of a translocator protein (25–27). The chaperone can then fold and attach to the translocator, producing a more rigidly bound structure (Fig. 3*F*). Such a scenario is not without precedent. For example, the three TPR motif-containing domain of PP5 has been shown to become more structured when bound to its cognate binding

partner (the C terminus of Hsp90) (28). Moreover, studies on the six ankyrin repeat protein IκBα show it also has a weakly folded C terminus. Here, repeats five and six fold upon binding to their cognate partner (the transcription factor NF-κB) (29, 30). It has been shown that the function and lifetime within the cell of IκBα is critically linked to whether this region is structured via ligand binding or not (31). This exciting scenario has yet to be explored for the translocator chaperones.

In summary, these results show that the chaperone LcrH has a very flexible and weakly folded C terminus that is held together by its dimeric interface at the N terminus. We propose that such a flexible structure has biological relevance that at the very least is important in binding its cognate protein partners (twice the mass membrane translocator proteins). These results should be generally applicable to all translocator chaperones, as they all contain the same TPR motif fold.

Acknowledgments—We thank Dr. R. Rose and members of School of Biological and Chemical Sciences for critical reading of the manuscript and insightful discussions. We also thank Mudith Jayawardena for helping with LcrH expression, purification, and equilibrium denaturation experiments.

REFERENCES

1. Büttner, D. (2012) Protein export according to schedule. Architecture, assembly, and regulation of type III secretion systems from plant- and animal-pathogenic bacteria. *Microbiol. Mol. Biol. Rev.* **76,** 262–310
2. Marlovits, T. C., and Stebbins, C. E. (2010) Type III secretion systems shape up as they ship out. *Curr. Opin. Microbiol.* **13,** 47–52
3. Hauser, A. R. (2009) The type III secretion system of *Pseudomonas aeruginosa*: infection by injection. *Nat. Rev. Microbiol.* **7,** 654–665
4. Matteï, P. J., Faudry, E., Job, V., Izoré, T., Attree, I., and Dessen, A. (2011) Membrane targeting and pore formation by the type III secretion system translocon. *FEBS J.* **278,** 414–426
5. Mueller, C. A., Broz, P., and Cornelis, G. R. (2008) The type III secretion system tip complex and translocon. *Mol. Microbiol.* **68,** 1085–1095
6. Viboud, G. I., and Bliska, J. B. (2005) *Yersinia* outer proteins: role in modulation of host cell signaling responses and pathogenesis. *Annu. Rev. Microbiol.* **59,** 69–89
7. Job, V., Matteï, P. J., Lemaire, D., Attree, I., and Dessen, A. (2010) Structural basis of chaperone recognition of type III secretion system minor translocator proteins. *J. Biol. Chem.* **285,** 23224–23232
8. Lunelli, M., Lokareddy, R. K., Zychlinsky, A., and Kolbe, M. (2009) IpaB-IpgC interaction defines binding motif for type III secretion translocator. *Proc. Natl. Acad. Sci. U.S.A.* **106,** 9661–9666
9. Büttner, C. R., Sorg, I., Cornelis, G. R., Heinz, D. W., and Niemann, H. H. (2008) Structure of the *Yersinia enterocolitica* type III secretion translocator chaperone SycD. *J. Mol. Biol.* **375,** 997–1012
10. Edqvist, P. J., Bröms, J. E., Betts, H. J., Forsberg, A., Pallen, M. J., and Francis, M. S. (2006) Tetratricopeptide repeats in the type III secretion chaperone, LcrH. Their role in substrate binding and secretion. *Mol. Microbiol.* **59,** 31–44
11. Barta, M. L., Zhang, L., Picking, W. L., and Geisbrecht, B. V. (2010) Evidence for alternative quaternary structure in a bacterial type III secretion system chaperone. *BMC Struct. Biol.* **10,** 21
12. Schreiner, M., and Niemann, H. H. (2012) Crystal structure of the *Yersinia enterocolitica* type III secretion chaperone SycD in complex with a peptide of the minor translocator YopD. *BMC Struct. Biol.* **12,** 13
13. Adam, P. R., Patil, M. K., Dickenson, N. E., Choudhari, S., Barta, M., Geisbrecht, B. V., Picking, W. L., and Picking, W. D. (2012) Binding affects the tertiary and quaternary structures of the *Shigella* translocator protein IpaB and its chaperone IpgC. *Biochemistry* **51,** 4062–4071
14. Lokareddy, R. K., Lunelli, M., Eilers, B., Wolter, V., and Kolbe, M. (2010) Combination of two separate binding domains defines stoichiometry between type III secretion system chaperone IpgC and translocator protein IpaB. *J. Biol. Chem.* **285,** 39965–39975
15. Tan, Y. W., Yu, H. B., Sivaraman, J., Leung, K. Y., and Mok, Y. K. (2009) Mapping of the chaperone AcrH binding regions of translocators AopB and AopD and characterization of oligomeric and metastable AcrH-AopB-AopD complexes in the type III secretion system of *Aeromonas hydrophila*. *Protein Sci.* **18,** 1724–1734
16. Scott, D. J., Harding, S. E., and Rowe, A. J. (2005) in *UltraScan. A Comprehensive Data Analysis Software Package for Analytical Ultracentrifugation Experiments* (Demeler, B., ed) Royal Society of Chemistry, Cambridge, UK
17. Hayes, D. B., Laue, T., and Philo, J. (1998) *Sednterp,* University of New Hampshire, Durham
18. Riley, P. W., Cheng, H., Samuel, D., Roder, H., and Walsh, P. N. (2007) Dimer dissociation and unfolding mechanism of coagulation factor XI Apple 4 domain. Spectroscopic and mutational analysis. *J. Mol. Biol.* **367,** 558–573
19. Rumfeldt, J. A., Galvagnion, C., Vassall, K. A., and Meiering, E. M. (2008) Conformational stability and folding mechanisms of dimeric proteins. *Prog. Biophys, Mol. Biol.* **98,** 61–84
20. Main, E. R., Lowe, A. R., Mochrie, S. G., Jackson, S. E., and Regan, L. (2005) A recurring theme in protein engineering: the design, stability, and folding of repeat proteins. *Curr. Opin. Struct. Biol.* **15,** 464–471
21. Main, E. R., Jackson, S. E., and Regan, L. (2003) The folding and design of repeat proteins: reaching a consensus. *Curr. Opin. Struct. Biol.* **13,** 482–489
22. Phillips, J. J., Javadi, Y., Millership, C., and Main, E. R. (2012) Modulation of the multistate folding of designed TPR proteins through intrinsic and extrinsic factors. *Protein Sci.* **21,** 327–338
23. Javadi, Y., and Main, E. R. (2009) Exploring the folding energy landscape of a series of designed consensus tetratricopeptide repeat proteins. *Proc. Natl. Acad. Sci. U.S.A.* **106,** 17383–17388
24. Main, E. R., Stott, K., Jackson, S. E., and Regan, L. (2005) Local and long range stability in tandemly arrayed tetratricopeptide repeats. *Proc. Natl. Acad. Sci. U.S.A.* **102,** 5721–5726
25. Levy, Y., Onuchic, J. N., and Wolynes, P. G. (2007) Fly-casting in protein-DNA binding. Frustration between protein folding and electrostatics facilitates target recognition. *J. Am. Chem. Soc.* **129,** 738–739
26. Perham, M., Chen, M., Ma, J., and Wittung-Stafshede, P. (2005) Unfolding of heptameric co-chaperonin protein follows "fly casting" mechanism: observation of transient nonnative heptamer. *J. Am. Chem. Soc.* **127,** 16402–16403
27. Shoemaker, B. A., Portman, J. J., and Wolynes, P. G. (2000) Speeding molecular recognition by using the folding funnel: the fly-casting mechanism. *Proc. Natl. Acad. Sci. U.S.A.* **97,** 8868–8873
28. Cliff, M. J., Williams, M. A., Brooke-Smith, J., Barford, D., and Ladbury, J. E. (2005) Molecular recognition via coupled folding and binding in a TPR domain. *J. Mol. Biol.* **346,** 717–732
29. Lamboy, J. A., Kim, H., Lee, K. S., Ha, T., and Komives, E. A. (2011) Visualization of the nanospring dynamics of the IκBα ankyrin repeat domain in real time. *Proc. Natl. Acad. Sci. U.S.A.* **108,** 10178–10183
30. Truhlar, S. M., Torpey, J. W., and Komives, E. A. (2006) Regions of IκBα that are critical for its inhibition of NF-κB. DNA interaction fold upon binding to NF-κB. *Proc. Natl. Acad. Sci. U.S.A.* **103,** 18951–18956
31. O'Dea, E. L., Barken, D., Peralta, R. Q., Tran, K. T., Werner, S. L., Kearns, J. D., Levchenko, A., and Hoffmann, A. (2007) A homeostatic model of IκB metabolism to control constitutive NF-κB activity. *Mol. Syst. Biol.* **3,** 111
32. Deu, E., and Kirsch, J. F. (2007) The unfolding pathway for apo *Escherichia coli* aspartate aminotransferase is dependent on the choice of denaturant. *Biochemistry* **46,** 5810–5818
33. Doyle, S. M., Braswell, E. H., and Teschke, C. M. (2000) SecA folds via a dimeric intermediate. *Biochemistry* **39,** 11667–11676
34. Grimsley, J. K., Scholtz, J. M., Pace, C. N., and Wild, J. R. (1997) Organophosphorus hydrolase is a remarkably stable enzyme that unfolds through a homodimeric intermediate. *Biochemistry* **36,** 14366–14374
35. Mei, G., Di Venere, A., Buganza, M., Vecchini, P., Rosato, N., and Finazzi-Agro, A. (1997) Role of quaternary structure in the stability of dimeric proteins: the case of ascorbate oxidase. *Biochemistry* **36,** 10917–10922

LcrH, a Class II Chaperone from the Type Three Secretion System, Has a Highly Flexible Native Structure

Sunny K. Singh, Aimee L. Boyle and Ewan R. G. Main

J. Biol. Chem. 2013, 288:4048-4055.
doi: 10.1074/jbc.M112.395889 originally published online December 11, 2012